Showcasing research from Professor Ju Li's laboratory, Massachusetts Institute of Technology, Cambridge, US.

Upcycling spent medium-Ni cathodes *via* novel liquified salt sourcing

We present a direct upcycling strategy that converts spent medium-Ni cathodes into Ni-rich, single-crystalline cathode materials using liquified eutectic salt chemistry. A transient quasi-liquid phase, formed from $LiOH–LiNO_3$ and $Ni(NO_3)_2 \cdot 6H_2O$ under planetary centrifugal mixing, enables uniform precursor diffusion and microstructural reconstruction. This process suppresses rock-salt phase formation and significantly enhances electrochemical performance, delivering improved cycling stability and rate capability. The scalable, energy-efficient method minimizes greenhouse gas emissions and energy consumption, offering a sustainable and transformative approach to spent battery and next-generation cathode production.

Image reproduced by permission of Moonsu Yoon from *Energy Environ. Sci.*, 2025, **18**, 5902.

ROYAL SOCIETY OF CHEMISTRY

rsc.li/ees

Check for updates

Upcycling spent medium-Ni cathodes *via* novel liquified salt sourcing†

Moonsu Yoon, [ID] [ab] Jin-Sung Park, [acd] Weiyin Chen, [a] Yimeng Huang, [a] Tao Dai, [a] Yumin Lee, [b] Jungmin Shin, [b] Seungmi Lee, [b] Yongil Kim, [ID] [b] Dongsoo Lee, [b] Daiha Shin, [e] Jaephil Cho, [ID] [f] Yanhao Dong [ID] *[g] and Ju Li [ID] *[ah]

The rapid growth in lithium-ion battery technology underscores the urgent need for sustainable recycling to address the environmental and economic challenges of battery waste. This study introduces a liquified-salts-assisted upcycling approach to transform spent medium-Ni cathodes into high-performance single-crystalline Ni-rich cathodes. Utilizing the LiOH–LiNO$_3$–Ni(NO$_3$)$_2$·6H$_2$O eutectic, this method leverages planetary centrifugal mixing to create a liquid-like environment for accelerated elemental diffusion and microstructural refinement. The *in situ* liquefaction of these salts ensures seamless precursor integration, achieving compositional uniformity and minimizing impurity formation. Compared to conventional solid-state methods, our method significantly suppresses rock-salt phase formation, and improves electrochemical performance with superior cycling stability and rate capability. The environmental and economic advantages of our approach highlight its potential to reduce greenhouse gas emissions and energy consumption. This scalable, energy-efficient strategy provides a transformative solution for battery waste management, paving the way for the sustainable production of next-generation cathode materials.

Broader context

The rapid expansion of lithium-ion battery usage, driven by electric vehicles and renewable energy storage, has raised significant environmental and economic concerns regarding the management of end-of-life batteries. Traditional recycling methods, such as hydrometallurgy and pyrometallurgy, often involve environmentally harmful processes, high energy consumption, and substantial waste generation. This research introduces a novel liquified-salts-assisted upcycling strategy for transforming spent medium-nickel cathodes into high-performance, Ni-rich cathode materials. By utilizing a eutectic mixture of LiOH–LiNO$_3$ and Ni(NO$_3$)$_2$·6H$_2$O, combined with planetary centrifugal mixing, this method significantly reduces energy consumption, minimizes greenhouse gas emissions, and achieves superior electrochemical performance compared to conventional recycling techniques. This scalable and sustainable approach addresses critical environmental issues associated with battery waste and provides a practical pathway toward the circular economy, supporting the sustainable growth of next-generation battery technologies.

Introduction

The growing global demand for carbon-neutral energy has made lithium-ion batteries (LIBs) indispensable for large-scale energy storage, particularly in applications such as electric vehicles and grid systems.[1–3] The market for rechargeable LIBs was valued at approximately \$46 billion in 2022, and is projected to reach \$190 billion by 2032, growing at an annual rate of nearly 15%.[4,5] With a typical lifespan of less than 10 years, the foreseeable staggering accumulation of

[a] Department of Nuclear Science and Engineering, Massachusetts Institute of Technology, Cambridge, Massachusetts, 02139, USA. E-mail: liju@mit.edu

[b] Department of Chemical, Biological and Battery Engineering, Gachon University, Seongnam, 13120, Republic of Korea

[c] Department of Materials Science and Engineering, Ajou University, Suwon, 16499, Republic of Korea

[d] Department of Energy Systems Research, Ajou University, Suwon, 16499, Republic of Korea

[e] Metropolitan Seoul Center, Korea Basic Science Institute, Seoul, 03759, Republic of Korea

[f] Department of Energy Engineering, School of Energy and Chemical Engineering, Ulsan National Institute of Science and Technology, Ulsan, 44919, Republic of Korea

[g] State Key Laboratory of New Ceramics and Fine Processing, School of Materials Science and Engineering, Tsinghua University, Beijing, 100084, China. E-mail: dongyanhao@tsinghua.edu.cn

[h] Department of Material Science and Engineering, Massachusetts Institute of Technology, Cambridge, Massachusetts, 02139, USA

† Electronic supplementary information (ESI) available. See DOI: https://doi.org/10.1039/d5ee01086a

5902 | *Energy Environ. Sci.*, 2025, **18**, 5902–5912

This journal is © The Royal Society of Chemistry 2025

spent/degraded LIBs raises significant concerns about sustainability. There is an urgent need for advanced recycling technologies and infrastructure to manage such waste.[6,7] The primary focus in spent LIB recycling is on cathode materials, which constitute more than one-third of the LIB total weight and nearly half of its cost.[8,9] In particular, high-value metallic elements (Ni, Co, and Li), in ternary cathode materials NCM ($LiNi_xCo_yMn_zO_2$, $x + y + z = 1$), are unevenly distributed globally, imposing significant environmental and social burdens for mining and transportation.[10–13] Effective closed-loop recycling strategies are essential to mitigate the environmental impact of battery wastes and reduce reliance on resource-intensive mining practices.

As a cutting-edge method, "upcycling" has emerged to offset the recycling cost by ensuring higher value and superior performance. Direct conversion from Ni-lean to higher-energy-density Ni-rich compositions is gaining significant attention, as medium-Ni NCM with $x \leq 0.5$ were the first ones mass-produced and will be the first ones to retire among the ternary cathode family.[14–16] One of the most practiced upcycling approaches is *via* hydrometallurgy, which reclaims the simple metals, oxides, or their salts from the spent cathode materials.[17–19] It typically involves destroying the entire cathode microstructure in acidic leaching solutions at mild temperatures, enabling the recovery of valuable metal elements (including Li) in the form of salt precursors (*e.g.*, Li_2CO_3 and $M(SO_4) \cdot xH_2O$, M = Ni, Co, and Mn). However, a massive amount of wastewater is inevitably generated during the neutralization process of the strong acid solutions, which continues to raise environmental and safety concerns. Alternatively, the pyrometallurgical method, the most widely used approach in the field of heavy industry, can recover metal (Ni, Co, and Mn) alloys through high-temperature ($>1200–1600$ °C) smelting and refining.[20,21] However, it must undergo complex steps to convert the alloys into high-purity Ni-rich precursor with micron-sized morphology. Furthermore, the destructive recycling methods of both hydrometallurgy and pyrometallurgy limit their output to lower-value products (such as salt precursors or alloys) derived from spent cathodes. Therefore, energy-consuming resynthesis steps are still required to recreate the high-value NCM cathodes with optimal stoichiometry and crystal structure.[22,23]

Direct upcycling offers a non-destructive alternative by utilizing spent cathode powders as precursors in the subsequent resynthesis of cathodes.[24–26] By supplying the lost Li and additional Ni to the spent Ni-lean cathodes, Ni-rich cathode materials can be directly synthesized to build new LIBs. Despite requiring pre-treatment steps, such as the removal of organic residues (electrolytes, carbon additives, and binders) and quantification of Li deficiency, direct upcycling has distinct economic and environmental advantages over hydrometallurgy and pyrometallurgy approaches.[25] In the domain of direct upcycling, the solid-state synthesis method is particularly noteworthy for its simplicity and compatibility with the conventional manufacturing process for TM-based (*e.g.* layered-/spinel-/olivine-types) cathode materials (Fig. 1). This method typically entails mechanically mixing a Li source (*e.g.*, LiOH) and a Ni source (*e.g.*, NiO or $Ni(OH)_2$) with the spent Ni-lean (or medium-Ni) cathode powders, followed by high-temperature

calcination (>800 °C). However, solid-state synthesis faces inherent limitations in achieving uniform contact between the solid precursors.[27] Mechanical mixing often necessitates prolonged high-energy ball-milling (sometimes lasting hundreds of hours at thousands of rounds per minute), to deagglomerate the micro-sized secondary particles into nano-sized particles,[15,28,29] ensuring a more even contact between various precursors and spent cathode particles (Fig. 1). Without such energy-intensive preparation, diffusion pathways for Li and Ni during sintering remain restricted, often leading to the formation of impurity phases, such as Ni-rich rock-salt and residual Li compounds on the cathode surface. These impurities potentially degrade the electrochemical performance of re-synthesized Ni-rich cathodes. More importantly, the reliance on high-energy ball-milling poses a significant barrier to scaling up solid-state upcycling methods beyond the laboratory scale.[30,31] Given the challenges and limited industrial viability of the current direct upcycling method, developing a simple and scalable strategy is crucial to managing the upcoming end-of-life of widely employed LIBs.

Herein, we propose a novel liquified-salt-assisted upcycling approach that overcomes the limitations of conventional direct recycling and upcycling methods (Fig. 1). This strategy utilizes a eutectic mixture of LiOH–$LiNO_3$ along with $Ni(NO_3)_2 \cdot 6H_2O$ to accelerate the liquefaction and dispersion of precursor salts and spent cathode particles, creating a liquid-like environment during planetary centrifugal mixing. The *in situ* melting of eutectic Li-salts and liquified nitrates promotes rapid dissolution and dispersion, and provides a seamless integration of elemental replenishment and microstructural refinement, thus enabling the transformation of spent medium-Ni cathodes into high-performance Ni-rich cathodes with single-crystalline morphology. Beyond its environmental and economic advantages, this scalable and energy-efficient technique redefines the potential of upcycling, paving the way for sustainable LIB waste management and the development of next-generation high-energy-density cathode materials.

Results and discussion

Ni-enriched precursors sourced from waste cathodes and eutectic liquified salts

We chose a spent $LiNi_{0.5}Co_{0.2}Mn_{0.3}O_2$ (NCM523) cathode as the precursors for upcycling due to its prominence as a commercial cathode material in the past decade. Following mild heat treatment (~ 400 °C, 20 min) and manual scraping, we separated and collected the spent NCM523 powders (Li deficient, with chemical formula $Li_xNi_{0.5}Co_{0.2}Mn_{0.3}O_2$ and $x \approx 0.8$) from cathode electrodes, as detailed in Fig. S1 and S2 (ESI†). To demonstrate the liquified-salts-assisted upcycling method, we employed a planetary centrifugal mixer (THINKY ARE-310, maximum capacity: ~ 310 g)—a device commonly used for mixing, dispersing, deaerating and slurry preparation—in the present study. Targeting a Ni-rich layered cathode $Li_{1.0}Ni_{0.80}Co_{0.08}Co_{0.12}O_2$ (NCM811) as the final product, we mixed spent

This journal is © The Royal Society of Chemistry 2025

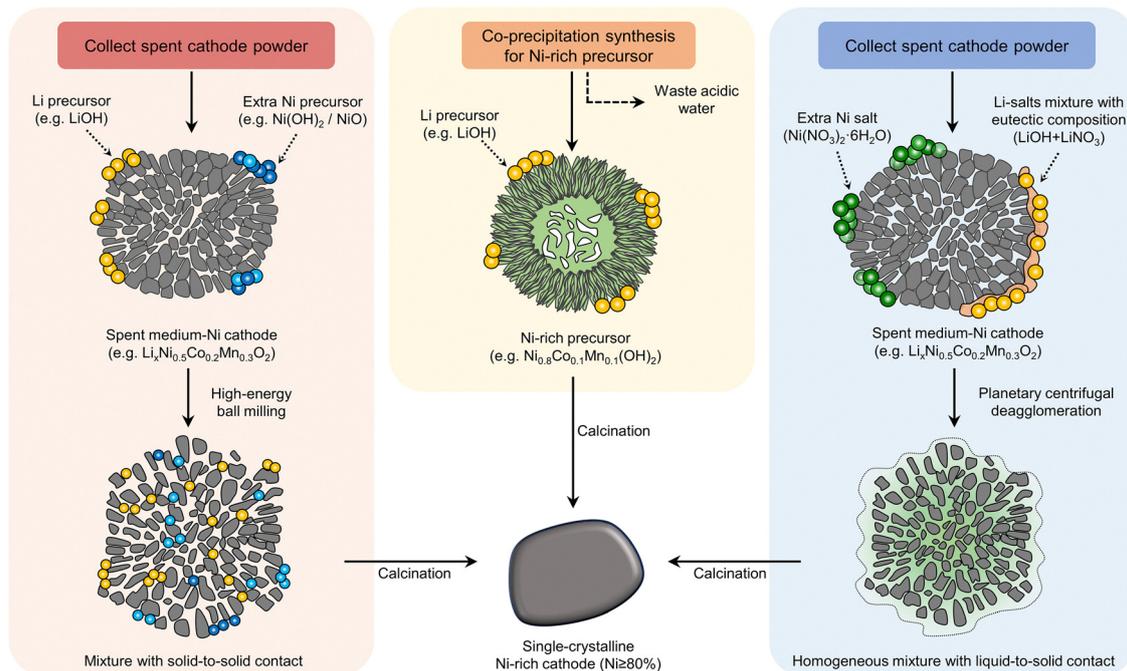*Energy Environ. Sci.*, 2025, **18**, 5902–5912 | 5903

Fig. 1 Schematic comparison of three methods to synthesize Ni-rich single-crystalline cathodes. A conventional solid-state approach involves collecting spent medium-Ni cathode powder (*e.g.*, $Li_xNi_{0.5}Co_{0.2}Mn_{0.3}O$) and adding Li and Ni precursors (*e.g.*, LiOH and $Ni(OH)_2$ or NiO). High-energy ball milling is employed to promote solid-to-solid contact among particles, forming a solid-state mixture that undergoes calcination to yield a Ni-rich cathode (left). The co-precipitation synthesis route fabricates a Ni-rich precursor (*e.g.*, $Ni_{0.8}Co_{0.1}Mn_{0.1}(OH)_2$) mixing with LiOH, followed by calcination. This method provides compositional homogeneity, but it generates acidic wastewater as a by-product (middle). The liquified-salts-assisted upcycling approach utilizes a eutectic mixture of $LiNO_3$–LiOH with additional $Ni(NO_3)_2·6H_2O$ as a Ni source. Planetary centrifugal deagglomeration promotes liquid-to-solid contact between the liquified salts and spent cathode powder, resulting in a homogeneously distributed mixture and high-quality single-crystalline Ni-rich cathode (right).

NCM523 with $LiOH$–$LiNO_3$ (40:60 molar ratio at the eutectic composition) and additional $Ni(NO_3)_2·6H_2O$ (to increase the Ni concentration from Ni 50% to Ni 80%) in the planetary centrifugal mixer at 2000 rpm without adding any grinding media. The amount of $LiOH$–$LiNO_3$ mixture was carefully calculated to account for both the Li deficiency in the spent NCM523 and the additional Li required for re-synthesizing the NCM811 layered cathode material (Table S1, ESI†).

As shown in Fig. 2(a)–(e), we observed distinct and rapid morphological changes in the mixture upon increasing mixing time. Initially, the raw chemicals exhibited distinct colors (green, white, and black) and morphologies (Fig. 2(a)), but after just 3 minutes of planetary centrifugal mixing, the mixture transformed into a uniform black color with wet powder morphology (Fig. 2(b)). Continued mixing for up to 6 min and 12 min further changed the mixture into a slurry-like form (Fig. 2(c)–(e)). This morphological evolution was well correlated with the microstructure observed *via* scanning electron microscopy (SEM). In comparison to the spent NCM523 cathode with secondary particle morphology, we found the primary particles of the NCM523 were well dispersed in the liquified matrix of eutectic $LiOH$–$LiNO_3$ and $Ni(NO_3)_2·6H_2O$ (Fig. 2(f) and (g) and Fig. S3, ESI†). The secondary particles became fully separated and embedded in a viscous and liquid-like matrix. Energy dispersive X-ray (EDS) mapping confirmed uniform elemental distributions (O, N and Ni; Fig. 2(h) and Fig. S3, ESI†),

indicating that the spent NCM523 and liquified salts, including eutectic $LiOH$–$LiNO_3$ and $Ni(NO_3)_2·6H_2O$ were uniformly integrated on a fine scale.

Along with the drastic microstructure changes, we observed intriguing phase evolution in the mixture through X-ray diffraction (XRD) analysis (Fig. 2(i)). The spent NCM523 in a slurry-like mixture remains in the layered structure before and after the planetary centrifugal mixing. However, the XRD peaks corresponding to $Ni(NO_3)_2·6H_2O$ gradually diminished, disappearing after 6 min of mixing (note that the XRD results are measured *ex situ* immediately after planetary centrifugal mixing, as shown in Fig. 2(i)). The behavior of the slurry-like mixture during planetary centrifugal mixing aligns with our previous study,[32,33] implying that the frictional forces between the mixed particles help reach an 'effective' temperature exceeding the melting points of $LiOH$–$LiNO_3$ eutectic (T_m = 183 °C) and $Ni(NO_3)_2·6H_2O$ (T_m = 56.7 °C) (Fig. S4, ESI†). Furthermore, we propose that the rapid transition from solid to a liquid-like phase within the 6 minutes of mixing could be facilitated by the presence of hydrates in the $Ni(NO_3)_2·6H_2O$ precursors. The hydrates are known to reduce the energy required for dissolution, thus promoting an early liquid-like environment and enhancing homogeneity in element distribution during planetary centrifugal mixing. Also, considering a density of 2.05 g cm^{-3} for $Ni(NO_3)_2·6H_2O$ and 4.80 g cm^{-3} for layered-type oxide, we estimated the volume ratio of the liquified nitrates to the oxide is about 11:1, which is sufficient to effectively wet and

5904 | *Energy Environ. Sci.*, 2025, **18**, 5902–5912

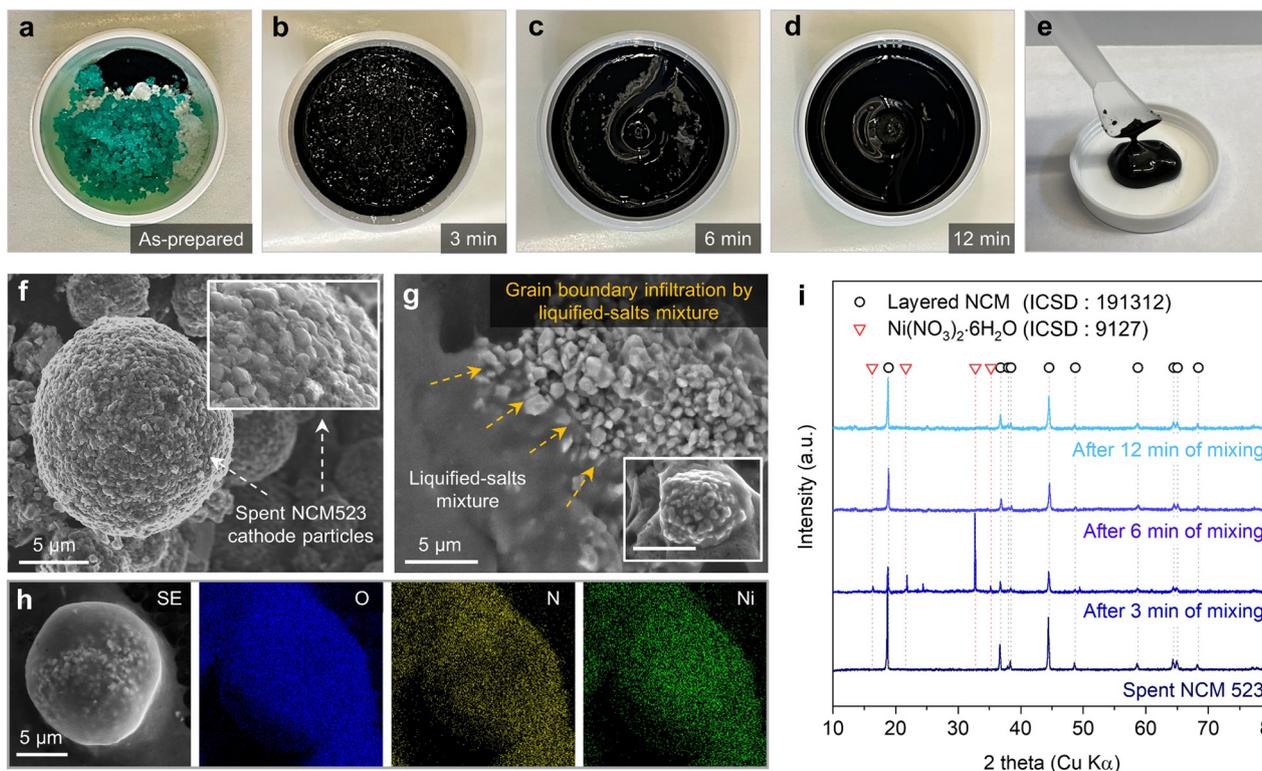This journal is © The Royal Society of Chemistry 2025

Fig. 2 Morphological and structural evolution of spent NCM523 during the liquified-salts-assisted upcycling process. (a)–(e) Digital images of the spent NCM523 cathode material as it undergoes liquified-salts-assisted upcycling through planetary centrifugal mixing. (a) The initial state of the dry, as-prepared mixture, followed by stages at (b) 3 min, (c) 6 min and (d) and (e) 12 min of mixing spent NCM523 powder with $LiOH-LiNO_3$ (as Li source) and $Ni(NO_3)_2 \cdot 6H_2O$ (as Ni source). (f) and (g) SEM images of the powder mixture in the as-prepared state and after 12 min mixing. (h) Secondary-electron (SE) image and EDS mapping of O, N, and Ni of the powder mixture after 12 min of mixing. (i) XRD patterns of the mixture of spent NCM523 powder with $LiOH-LiNO_3$ and $Ni(NO_3)_2 \cdot 6H_2O$ at different mixing times.

fully separate the primary particles of the spent NCM523 cathode.[34] As a result, the liquefaction of the $LiOH-LiNO_3-Ni(NO_3)_2 \cdot 6H_2O$ mixture accelerated by multiple hydrates enables the deagglomeration of spent NCM523 particles, and this allows them to become separately embedded within the liquified matrix, thus fostering intimate contacts among precursors and the formation of a dense colloidal suspension.

Chemical and microstructural upcycling

Fig. 3 compares the microstructure, phase composition, and elemental distribution between Ni-rich cathodes (target composition: $Li_{1.0}Ni_{0.80}Co_{0.08}Mn_{0.12}O_2$) re-synthesized *via* a conventional solid-state direct upcycling method (SS-NCM) and those processed by the new liquified-salts-assisted upcycling method (LS-NCM). We selected SS-NCM as a reference because it is conventionally re-synthesized by using $Ni(OH)_2$ and LiOH, providing a suitable baseline for evaluating the benefits introduced by liquified-salts-assisted upcycling. In the synthesis process of SS-NCM, we used a lab-scale mechanical mixer with additional hand grinding instead of high-energy ball-milling to identify the significant effect of the mixer type on the performance of the cathode material. Fig. 3(a) and (d) depict the morphology of SS-NCM and LS-NCM cathodes, respectively, as observed by SEM. Despite their relatively small primary particle

size, SS-NCM particles are heavily agglomerated as consistent with typical microstructural features for solid-state synthesis (Fig. S5, ESI†). In contrast, LS-NCM has more uniformly distributed micro-sized particles and fewer agglomerates, indicating that the liquified-salts-assisted method facilitates more uniform particle dispersion and a smoother surface morphology. The less agglomerated LS-NCM than SS-NCM is further supported by smaller D_{50} in particle size distribution and smaller surface area of the former (Table S2 and Fig. S6, ESI†). The enhancement in particle uniformity can provide consistency in the quality of the electrode fabrication process, and also reduces inconsistency in electrochemical reactions.

In addition, with the morphology difference between SS-NCM and LS-NCM, we also revealed that liquified-salts contribute significantly to structural modification. Through high-angle annular dark-field scanning transmission electron microscopy (HAADF-STEM) and high-resolution transmission electron microscopy (HR-TEM) analysis, we observed an evolution of multiple inter-granular cracks with extensive void defects and rock-salt structure in spent NCM523, which is consistent with a deteriorated NCM523 cathode (Fig. S7, ESI†).[35,36] After the solid-state upcycling process, the HAADF-STEM images of SS-NCM show a rock-salt structure with ~10 nm thickness covering the combined layered and rock-salt structure beneath, and the corresponding

This journal is © The Royal Society of Chemistry 2025

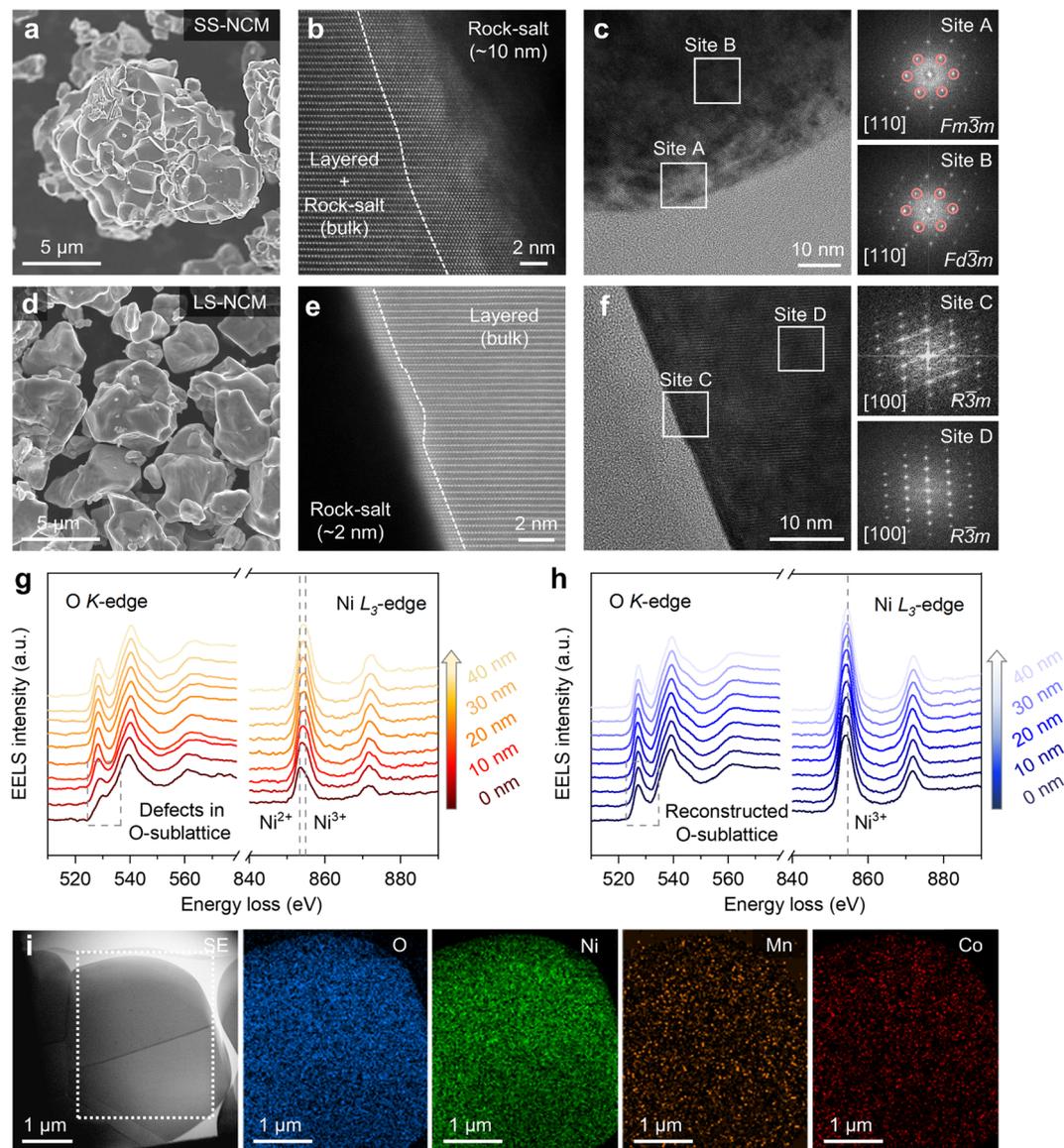*Energy Environ. Sci.*, 2025, **18**, 5902–5912 | **5905**

Fig. 3 Chemical and structural characterizations of micro-sized LS-NCM. (a)–(h) Comparative microstructural, crystallographic, and elemental analysis of SS-NCM and LS-NCM cathodes. (a)–(c) SEM images, HAADF-STEM, and HR-TEM with FFT patterns of SS-NCM. (d)–(f) SEM images, HAADF-STEM, and HR-TEM with FFT patterns of LS-NCM. (g) and (h) EELS line scan profile of SS-NCM (red, left) and LS-NCM (blue, right) measured from the outer surface (0 nm) to inner surface of 40 nm depth. (i) TEM image and EDS mapping results of LS-NCM in the corresponding region.

region indicates $Fd\bar{3}m$ symmetry after fast-Fourier transform (FFT) in the HR-TEM results (Fig. 3(b) and (c)). In comparison, LS-NCM exhibited a notably thinner rock-salt layer ($Fm\bar{3}m$ symmetry) of approximately $\sim$2 nm along the sub-surface, and the bulk layered phase with $R\bar{3}m$ symmetry (Fig. 3(e) and (f)). From electron energy loss spectroscopy (EELS) measurements, severe Ni reduction (Ni^{3+} reduced to Ni^{2+} shown by the Ni L_3-edge) and defects in the oxygen sublattice (shown by the O K-edge) are observed in SS-NCM (Fig. 3(g)). In contrast, even at the surface of LS-NCM, Ni reduction and oxygen defects are rarely observed (Fig. 3(h), EELS scanning pathway on SS-NCM and LS-NCM are listed in Fig. S8, ESI†). The differences in sub-surface structure between SS-NCM and LS-NCM can be attributed to the manner in which the spent NCM523 powder is packed with Li- and Ni-based precursors. In

the solid-state synthesis of SS-NCM, solid–solid contacts predominate, thus defects (such as gradients in oxygen vacancies and Ni concentration) are likely to accumulate along the surfaces of the spent NCM523 particles, especially near the solid–solid junctions, due to the lack of a fluid medium. Indeed, through TEM-EDS analysis, we found localized Ni-rich regions on the surface and along the grain boundaries of SS-NCM particles (Fig. S9, ESI†). However, in LS-NCM synthesis, the early liquified salts can act as a diffusion medium that facilitates uniform distribution of Li and Ni ions and restoration of the lattice composition within the cathode particle matrix, thereby minimizing defects and reconstructing the sub-surface from rock-salt into a layered-structure. The compositional uniformity in LS-NCM can be further confirmed by Fig. 3(i) and Fig. S10 (ESI†), and these

surface and lattice structural features influence the electrochemical performance, especially for the cycling stability.

Accelerated phase evolution by liquified salt treatment

By using a high-temperature XRD (HT-XRD) technique, we next investigated the effect of liquified salts on phase evolution and structural restoration in LS-NCM during the high-temperature synthesis, and compared it with SS-NCM. Fig. 4 shows the contour maps of HT-XRD data and phase fractions of SS-NCM and LS-NCM measured at each temperature. For SS-NCM, the diffraction peaks corresponding to the spent NCM523 phase and $Ni(OH)_2$ are observed below 300 °C (Fig. 4(a)). As the temperature increases, partial decomposition of $Ni(OH)_2$ occurs and leads to the formation of the rock-salt phase (RS), evidenced by the $(200)_{RS}$ at $2\theta \approx 43.3°$ (Fig. S11a, ESI†). By 500 °C, the rock-salt phase becomes prominent and coexists with the layered structure (L), as indicated by the $(104)_L$ peak at $2\theta \approx 43.9°$. The layered structure gradually dominates the XRD pattern of SS-NCM as the temperature increases to ~800 °C. However, residual rock-salt domains persist, as evidenced by the negative peak shifts of $(102)_L$ toward $(111)_{RS}$ and $(104)_L$ toward $(200)_{RS}$ (Fig. 4(a) and Fig. S11a, ESI†).[37] The phase-fraction analysis in Fig. 4(b) also confirms a significant proportion of the rock-salt phase remains alongside the formation of

the layered phase. The persistence of the rock-salt phase at higher temperatures in SS-NCM highlights the limitations of the solid-state method for the upcycling process, particularly its inability to achieve complete structural restoration due to insufficient precursor distribution and limited ionic diffusion.

In contrast, the LS-NCM cathode synthesized using a eutectic mixture of $LiOH$–$LiNO_3$ and $Ni(NO_3)_2 \cdot 6H_2O$ as precursors exhibited a layered structure with significantly fewer impurities compared to SS-NCM (Fig. 4(c)). Below 300 °C, the diffraction peaks indicate the coexistence of spent NCM 523 and the $Ni(NO_3)_2$ precursors. As the temperature increases, $Ni(NO_3)_2$ decomposes into the rock-salt phase, initiating the formation of transient rock-salt phases between 300 °C and 500 °C. However, unlike in SS-NCM, the rock-salt phase in LS-NCM diminished rapidly beyond ~500 °C, and the diffraction peaks corresponding to the layered structure (*e.g.*, $(003)_L$, $(104)_L$) dominate the XRD pattern up to ~800 °C (Fig. S11b, ESI†). This observation fairly aligns with the TEM results of LS-NCM, which exhibit a thin rock-salt layer along the outer surface of LS-NCM with much less cation-mixing than in SS-NCM (Fig. S12 and Table S3, ESI†). The rapid recession of the rock-salt phase in LS-NCM can be attributed to nanoscale dispersion and intimate interfacial interaction facilitated by liquified salts. During SS-NCM synthesis, the limited contact between the solid
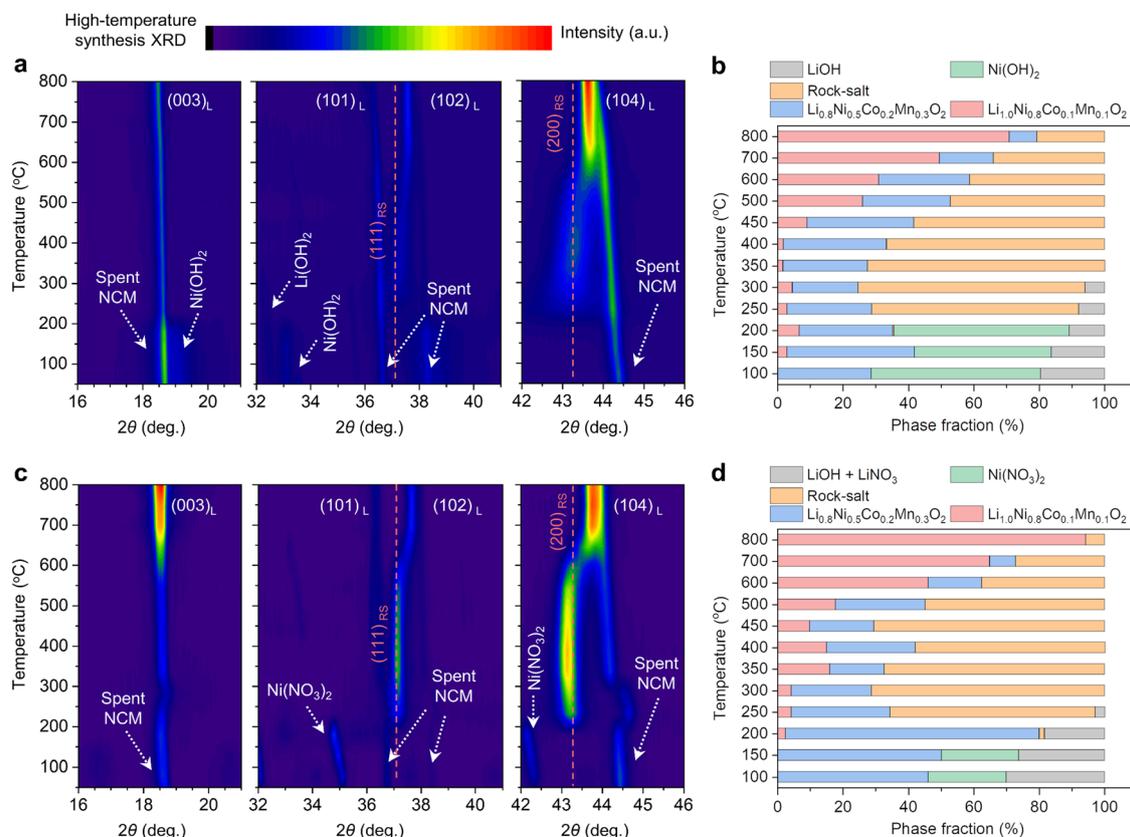

Fig. 4 Comparison of phase evolution in SS-NCM and LS-NCM during high-temperature annealing. (a) and (b) Contour maps of HT-XRD patterns of the mixture of spent NCM523 with LiOH and $Ni(OH)_2$, and phase fraction during the annealing process for SS-NCM synthesis. (c) and (d) Contour maps of the HT-XRD patterns of the mixture of spent NCM523 with a eutectic mixture of $LiOH$–$LiNO_3$ and $Ni(NO_3)_2$ and phase fraction during the high-temperature annealing process for LS-NCM synthesis.

precursors and spent NCM523 creates localized Ni-rich regions, where nickel is poorly incorporated into the lattice of spent NCM523. These regions stabilize the rock-salt phase, decelerating its complete conversion to the desired layered structure even at 800 °C. In contrast, in LS-NCM, the homogeneous dispersion of nickel and lithium elements *via* liquified-salts ensures that any rock-salt domains form as nanoscale clusters, almost fully surrounded by the spent NCM523 cathode. The nanoscale rock-salt domains exhibit physical properties analogous to those observed in systems undergoing melting-point depression.[38,39] The nanoscale rock-salt domains, with high surface-to-volume (S-to-V) ratio, render them thermodynamically unstable, leading to weakened atomic interactions at the surface and thus enabling their rapid dissolution into Li- and oxygen-rich environments.[40] The liquid phase formed by the eutectic Li-salts facilitates enhanced ion diffusion and promotes the reorganization of nickel, lithium, and oxygen within the cathode lattice.[41,42] As a result, larger and more stable spent NCM523 particles (with lower S-to-V ratio) grow at their expense, and the Ni in rock-salt phase are successfully incorporated into the layered structure as the temperature increases. Furthermore, TEM results confirm the growth of single-crystalline structures in LS-NCM, likely driven by Ostwald ripening, where smaller rock-salt domains dissolve and contribute to the growth of larger, stable layered particles with compositional uniformity.[32] The phase-fraction analysis in Fig. 4(d) corroborates these findings, showing the near-complete suppression of the rock-salt phase and the dominance of the Ni-rich layered structure in LS-NCM. The combination of liquified-salts-assisted synthesis and Ostwald ripening establishes LS-NCM as a superior approach for upcycling spent cathodes. By leveraging homogeneous precursor distribution and particle growth mechanisms, this method achieves structural restoration, compositional uniformity, and the suppression of undesirable phases such as rock-salt.

Electrochemical properties of upcycled cathodes

Next, we investigated the electrochemical performance of SS-NCM and LS-NCM as LIB cathodes. When the first cycle was performed at 0.1C (that is, the formation step; 1C defined as 200 mA g^{-1}) between 2.8 V and 4.3 V (*vs.* Li/Li$^+$), SS-NCM has a discharge capacity of 192 mA h g^{-1} and a first-cycle Coulombic efficiency (C.E.) of 84.9%. In comparison, LS-NCM has a slightly higher discharge capacity of 198 mA h g^{-1} and a higher first-cycle C.E. of 87.3% (Fig. 5(a), the first-cycle capacity and C.E. of reference NCM811 cathode materials are compared in Fig. S13, ESI†). The capacity improvement in both SS-NCM and LS-NCM compared to that of spent NCM523 can be ascribed to increased Ni concentration, leading to an extension of the Ni-redox reaction. Upon cycling at 0.5C charge/1.0C discharge for 100 cycles, LS-NCM has better capacity retention (94.1% for LS-NCM *vs.* 77.6% for SS-NCM) with more stable charge–discharge curves compared to SS-NCM (Fig. 5(b) and Fig. S13, ESI†). Furthermore, LS-NCM exhibits a better rate capability than SS-NCM (151 mA h g^{-1} for LS-NCM *vs.* 141 mA h g^{-1} for SS-NCM at 5C, Fig. 5(c) and Fig. S14, ESI†). To gain a better understanding of the improved cycling stability and rate capability, we conducted galvanostatic intermittent titration

technique (GITT) measurements with a titration current of 0.3C after the fifth and last (100th cycle in the total number of 0.5C/1.0C cycling) cycles. Here, we focused on the voltage loss during each relaxation step, which reflects ohmic and non-ohmic loss at each depth-of-discharge. As shown by the discharge profiles in Fig. 5(d), a more severe polarization developed in cycled SS-NCM than in cycled LS-NCM, and the average voltage loss was approximately 1.50 times greater in the former. The more detailed GITT analysis in Fig. S15 (ESI†) demonstrates a higher impedance growth in SS-NCM than in LS-NCM, mostly in the form of ohmic loss (which indicates degraded electron transport at the microstructure level, consistent with a wide range of rock-salt phase formation along the subsurface of SS-NCM); this is further supported by electrochemical impedance spectroscopy (EIS) measurements (Fig. S16, ESI†). In addition, compared with previous literature on Ni-rich cathodes synthesized from fresh or recycled precursors, LS-NCM shows compelling electrochemical performance even at wider voltage ranges from 2.8 to 4.4 V and from 2.8 to 4.5 V (*vs.* Li/Li$^+$) (Fig. 5(e) and Fig. S17, Table S4, ESI†). Lastly, to highlight the exceptional performance offered by the liquified-salts-assisted upcycling method, we tested SS-NCM and LS-NCM in 700 mA h pouch-type full-cells using a spherical graphite (Gr) anode and conducted long-term cycling in the range of 2.8–4.3 V at 25 °C (details of cell design in Table S5, ESI†). As shown in Fig. 5(f) and (g), LS-NCM has an impressive capacity retention of 88.1% (*vs.* 81.2% for SS-NCM) and a high C.E. at 1.0C/1.0C charge/discharge for 300 cycles (more detailed electrochemical performance data are provided in Fig. S18 and S19, ESI†). Given the stable cycling behavior of the Gr anode, the superior cycle life and reduced voltage decay in the LS-NCM/Gr full cell can be attributed to three factors: (i) a thinner and more uniform rock-salt layer that minimizes interfacial resistance and preserves cathode–electrolyte kinetics; (ii) suppressed electrolyte decomposition, leading to improved electrolyte integrity; and (iii) enhanced structural stability of LS-NCM that mitigates transition metal dissolution and subsequent anode-side degradation. These combined effects contribute to the overall reduction in impedance buildup and promote long-term cell durability. Therefore, facile elemental infusion through the intimate solid (spent NCM523) – liquid (Li-/Ni-salts) interface facilitates uniform microstructure modification, thereby resulting in improved electrochemical performance.

Economic and environmental analysis of liquified-salts-assisted upcycling

Using GREET 2020 and EverBatt 2020 software packages developed by Argonne National Laboratory,[43,44] we conducted a closed-loop life cycle analysis of LIBs, comparing the efficiencies of three upcycling methods depicted in Fig. 6 – pyrometallurgy, hydrometallurgy, and liquified-salts-assisted methods. The prospective cradle-to-gate life cycle assessments (LCA) are applied, consisting of the processes from the collection of individual intermediates from approximately 1.00 kg of spent LIBs (cradle) by different types of reactions to the production of cathode materials using these intermediates as the reaction
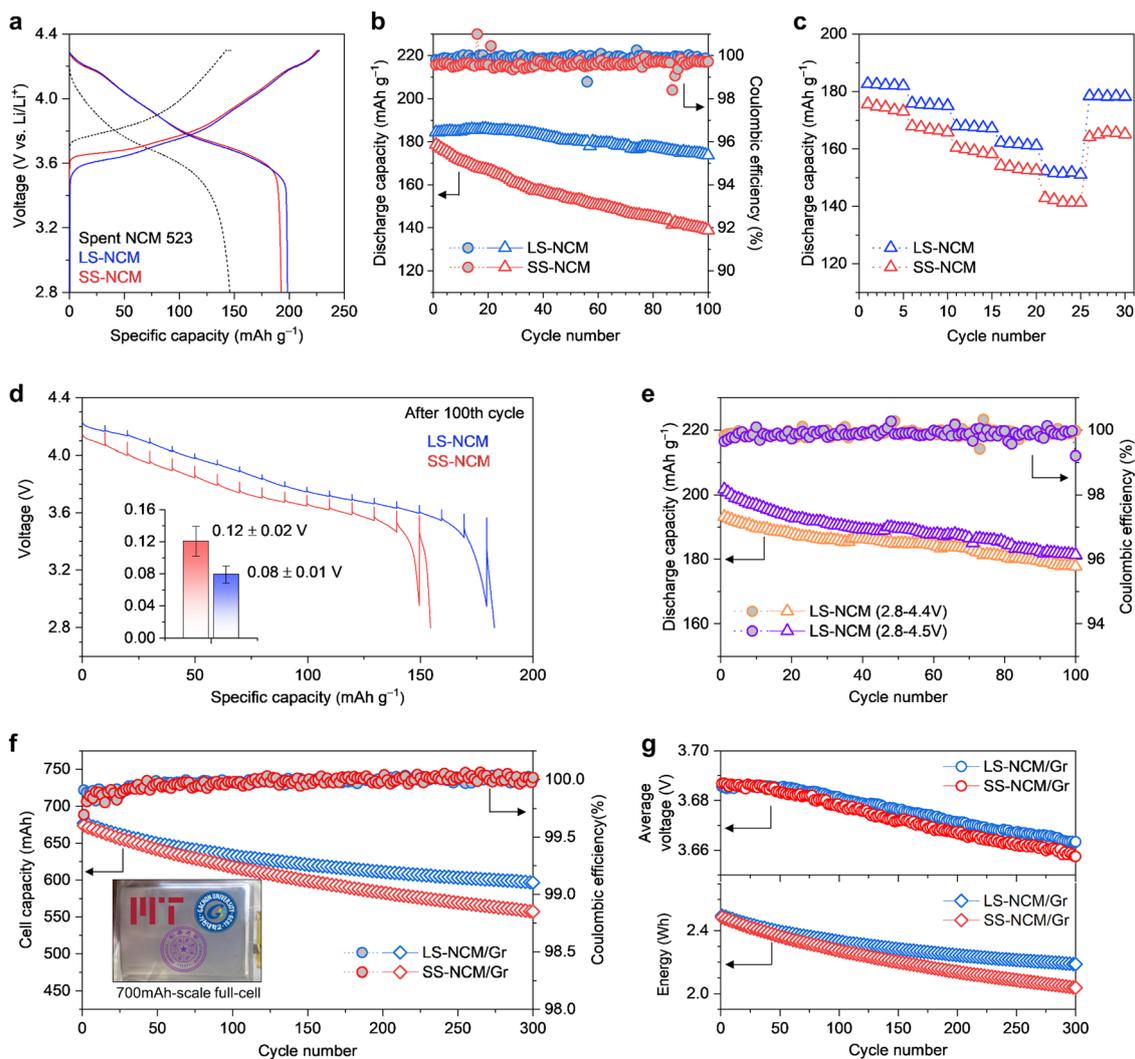
5908 | *Energy Environ. Sci.*, 2025, **18**, 5902–5912

This journal is © The Royal Society of Chemistry 2025

Fig. 5 Superior electrochemical performance of LS-NCM over SS-NCM. (a) Voltage–capacity curves of spent NCM523, LS-NCM and SS-NCM measured at the initial first cycle (formation step) with 0.1C in the voltage ranges of 2.8−4.3 V. (b) and (c) 0.5C charge−1.0C discharge cycling performance and rate tests of LS-NCM and SS-NCM after the formation step (1C defined as 200 mA g^{-1}). (d) Discharge curves of the GITT measurements conducted after the 100th cycle in (a). Inset: Average voltage loss and its standard deviation (raw data available in Fig. S15, ESI†) over different GITT steps. (e) Cycling performance of LS-NCM for 100 cycles at 0.5C charge−1.0C discharge in the voltage ranges of 2.8−4.4 V and 2.8−4.5 V (vs. Li/Li$^+$) at 25 °C (1C defined as 210 and 220 mA g^{-1} for 4.4 and 4.5 cut-off voltage, respectively). (f) and (g) Cycling performance of LS-NCM/Gr and SS-NCM/Gr full-cells at 1.0C in the range of 2.8−4.3 V at 25 °C. Inset: Photo of an assembled pouch cell.

precursors at the factory (gate). The use of spent NCM523 cathode material is considered a major source for the upcycling process, but its disposal (grave) is not considered. A more detailed discussion about LCA is shown in Note S1 (ESI†). Each of these upcycling pathways demonstrates distinct process flows, resource requirements, and environmental impacts (Fig. 6). As shown in Fig. 6(a)–(c), the liquified-salts-assisted method is the most environmentally sustainable option in this comparison, achieving high efficiency with minimal resource consumption. The use of low-temperature calcination and innovative mixing methods substantially reduces water and energy requirements and lowers greenhouse gas (GHG) emissions (Tables S6–S10 and Fig. S20, ESI†). The liquified-salts-assisted upcycling approach exhibits notably lower energy consumption (4.94 MJ per kg cell) and GHG emissions

(0.68 kg per kg cell) compared to traditional pyrometallurgical and hydrometallurgical recycling methods (Fig. 6(d) and Fig. S20, ESI†). Moreover, our method bypasses complex, water-intensive preprocessing steps by directly yielding usable cathode materials. Consequently, the simplified process can potentially lead to enhanced profitability through lower operational expenses, especially compared to destructive methods primarily aimed at recovering metallic precursors from spent cathodes (Fig. S21, ESI†). Indeed, among various direct recycling or upcycling strategies evaluated, our liquified-salts-assisted approach consistently demonstrates the lowest environmental impact (in terms of GHG emissions) and energy usage per kilogram of processed battery cells, alongside superior economic viability (Fig. S22, ESI†). It should be noted that the cost analysis presented here does not fully reflect the
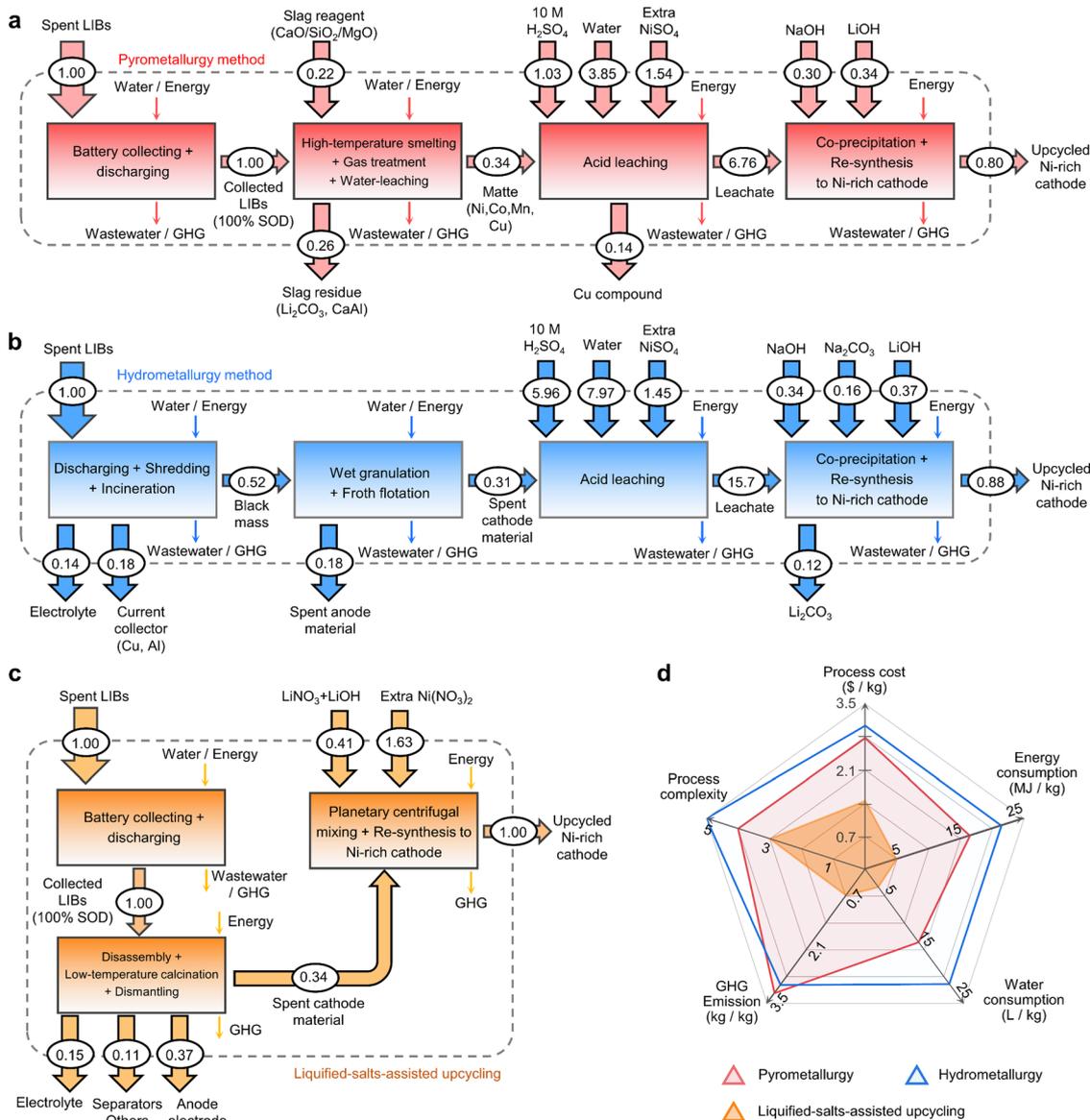
This journal is © The Royal Society of Chemistry 2025

Energy Environ. Sci., 2025, **18**, 5902–5912 | **5909**

Fig. 6 Economic and environmental analysis of liquified-salts-assisted upcycling method. (a)–(c) Process flow diagrams of various spent lithium-ion battery recycling routes, displaying the life cycle inventory including all considered inputs and outputs. Incidental inputs and outputs are shown with small arrows to differentiate them from explicit inputs and outputs. (a) Pyrometallurgy method, (b) hydrometallurgy method, and (c) liquified-salts-assisted upcycling method. The unit is kg for all material flow. (d) Spider diagram manifesting key features of upcycling methods regarding industrial viability (GHG: greenhouse gas).

complexities associated with industrial-scale deployment, particularly regarding precise quantification of additional Li and Ni, and atmospheric control, due to current methodological limitations. Nevertheless, the compelling combination of minimal energy consumption, lowest GHG emissions, and competitive upcycling costs positions our method as a promising candidate for real-world industrial application. Our approach aligns with the growing demand for cost-effective, low-environmental-impact LIBs upcycling solutions. With increased interest in cathode materials possessing high-Ni concentration and low Co contents, such as $LiNi_{0.90}Co_{0.05}Mn_{0.05}O_2$ and $LiNi_{0.80}Co_{0.15}Al_{0.05}O_2$, more economically-efficient recycling with

eco-friendly benefits might be attainable using the liquified-salts-assisted method.

Author contributions

M. Y., Y. D., and J. L. conceived the project. M. Y. and Y. D. designed the experiments and analyzed the data. M. Y. and J. P. synthesized the materials and conducted electrochemical testing. W. C. conducted SEM and *ex situ* XRD measurements. D. S. conducted *in situ* XRD measurements. Y. H. and T. D. analyzed the TEM data. Y. L., J. S. and S. L. designed and assembled

5910 | *Energy Environ. Sci.*, 2025, **18**, 5902–5912

This journal is © The Royal Society of Chemistry 2025

pouch-type full-cells and conducted electrochemical tests. M. Y. calculated the economic and environmental impacts of the upcycling process using EverBatt 2020 and GREET 2020. J. C. contributed to the evaluation and analysis of the study. M. Y., Y. D. and J. L. wrote the paper. All authors discussed and contributed to the writing.

Data availability

Data generated and analyzed in the present work are available in the manuscript and the ESI.†

Conflicts of interest

This work used the methodology reported for the US Provisional Patent Application (US 63/484,989), filed by the MIT Technology Licensing office for our previous work.[32] The authors declare no other competing interests.

Acknowledgements

References

1 W. Li, E. M. Erickson and A. Manthiram, *Nat. Energy*, 2020, **5**, 26–34.

2 R. E. Ciez and J. F. Whitacre, *Nat. Sustainability*, 2019, **2**, 148–156.

3 M. Armand and J. M. Tarascon, *Nature*, 2008, **451**, 652–657.

4 H.-H. Ryu, H. H. Sun, S.-T. Myung, C. S. Yoon and Y.-K. Sun, *Energy Environ. Sci.*, 2021, **14**, 844–852.

5 International Energy Agency (IEA), Global EV Outlook 2023, 2023.

6 X. Ma, M. Chen, Z. Zheng, D. Bullen, J. Wang, C. Harrison, E. Gratz, Y. Lin, Z. Yang, Y. Zhang, F. Wang, D. Robertson, S.-B. Son, I. Bloom, J. Wen, M. Ge, X. Xiao, W.-K. Lee, M. Tang, Q. Wang, J. Fu, Y. Zhang, B. C. Sousa, R. Arsenault, P. Karlson, N. Simon and Y. Wang, *Joule*, 2021, **5**, 2955–2970.

7 Y. Huang and J. Li, *Adv. Energy Mater.*, 2022, **12**, 2202197.

8 M. Fan, X. Chang, Y.-J. Guo, W.-P. Chen, Y.-X. Yin, X. Yang, Q. Meng, L.-J. Wan and Y.-G. Guo, *Energy Environ. Sci.*, 2021, **14**, 1461–1468.

9 X. Xiao, L. Wang, Y. Wu, Y. Song, Z. Chen and X. He, *Energy Environ. Sci.*, 2023, **16**, 2856–2868.

10 J. Baars, T. Domenech, R. Bleischwitz, H. E. Melin and O. Heidrich, *Nat. Sustainability*, 2021, **4**, 71–79.

11 Y. Tao, C. D. Rahn, L. A. Archer and F. You, *Sci. Adv.*, 2021, **7**, eabi7633.

12 W. Chen, J. Chen, K. V. Bets, R. V. Salvatierra, K. M. Wyss, G. Gao, C. H. Choi, B. Deng, X. Wang, J. T. Li, C. Kittrell, N. La, L. Eddy, P. Scotland, Y. Cheng, S. Xu, B. Li, M. B. Tomson, Y. Han, B. I. Yakobson and J. M. Tour, *Sci. Adv.*, 2023, **9**, eadh5131.

13 G. Harper, R. Sommerville, E. Kendrick, L. Driscoll, P. Slater, R. Stolkin, A. Walton, P. Christensen, O. Heidrich, S. Lambert, A. Abbott, K. Ryder, L. Gaines and P. Anderson, *Nature*, 2019, **575**, 75–86.

14 T. Wang, H. Luo, J. Fan, B. P. Thapaliya, Y. Bai, I. Belharouak and S. Dai, *iScience*, 2022, **25**, 103801.

15 X. Ma, J. Hou, P. Vanaphuti, Z. Yao, J. Fu, L. Azhari, Y. Liu and Y. Wang, *Chem*, 2022, **8**, 1944–1955.

16 G. Qian, Z. Li, Y. Wang, X. Xie, Y. He, J. Li, Y. Zhu, S. Xie, Z. Cheng, H. Che, Y. Shen, L. Chen, X. Huang, P. Pianetta, Z.-F. Ma, Y. Liu and L. Li, *Cell Rep. Phys. Sci.*, 2022, **3**(2), 100741.

17 X. Zhang, Y. Bian, S. Xu, E. Fan, Q. Xue, Y. Guan, F. Wu, L. Li and R. Chen, *ACS Sustainable Chem. Eng.*, 2018, **6**, 5959–5968.

18 Y. Zheng, S. Wang, Y. Gao, T. Yang, Q. Zhou, W. Song, C. Zeng, H. Wu, C. Feng and J. Liu, *ACS Appl. Energy Mater.*, 2019, **2**, 6952–6959.

19 Y. Yao, M. Zhu, Z. Zhao, B. Tong, Y. Fan and Z. Hua, *ACS Sustainable Chem. Eng.*, 2018, **6**, 13611–13627.

20 X. Hu, E. Mousa, Y. Tian and G. Ye, *J. Power Sources*, 2021, **483**, 228936.

21 J. B. Dunn, L. Gaines, J. C. Kelly, C. James and K. G. Gallagher, *Energy Environ. Sci.*, 2015, **8**, 158–168.

22 W. Chu, Y. Zhang, X. Chen, Y. Huang, H. Cui, M. Wang and J. Wang, *J. Power Sources*, 2020, **449**, 227567.

23 S. Ko, J. Choi, J. Hong, C. Kim, U. Hwang, M. Kwon, G. Lim, S. S. Sohn, J. Jang, U. Lee, C. B. Park and M. Lee, *Energy Environ. Sci.*, 2024, **17**, 4064–4077.

24 Z. Xiao, Y. Yang, Y. Li, X. He, J. Shen, L. Ye, F. Yu, B. Zhang and X. Ou, *Small*, 2024, 2309685.

25 J. Wang, J. Ma, Z. Zhuang, Z. Liang, K. Jia, G. Ji, G. Zhou and H.-M. Cheng, *Chem. Rev.*, 2024, **124**, 2839–2887.

26 Y. Lan, X. Li, G. Zhou, W. Yao, H.-M. Cheng and Y. Tang, *Adv. Sci.*, 2024, **11**, 2304425.

27 A. Banik, T. Famprikis, M. Ghidiu, S. Ohno, M. A. Kraft and W. G. Zeier, *Chem. Sci.*, 2021, **12**, 6238–6263.

28 X. Meng, J. Hao, H. Cao, X. Lin, P. Ning, X. Zheng, J. Chang, X. Zhang, B. Wang and Z. Sun, *Waste Manage.*, 2019, **84**, 54–63.

29 Y. Han, Y. You, C. Hou, X. Xiao, Y. Xing and Y. Zhao, *J. Electrochem. Soc.*, 2021, **168**, 040525.

30 J. Jeswiet and A. Szekeres, *Procedia CIRP*, 2016, **48**, 140–145.

31 G. Ji, D. Tang, J. Wang, Z. Liang, H. Ji, J. Ma, Z. Zhuang, S. Liu, G. Zhou and H.-M. Cheng, *Nat. Commun.*, 2024, **15**, 4086.

32 M. Yoon, Y. Dong, Y. Huang, B. Wang, J. Kim, J.-S. Park, J. Hwang, J. Park, S. J. Kang, J. Cho and J. Li, *Nat. Energy*, 2023, **8**, 482–491.

33 H. Yang, C.-A. Wang and Y. Dong, *Adv. Powder Mater.*, 2024, **3**, 100185.

This journal is © The Royal Society of Chemistry 2025

Energy Environ. Sci., 2025, **18**, 5902–5912 | 5911

34 L. Berger and S. A. Friedberg, *J. Appl. Phys.*, 1965, **36**, 1158.

35 S. Klein, P. Bärmann, T. Beuse, K. Borzutzki, J. E. Frerichs, J. Kasnatscheew, M. Winter and T. Placke, *ChemSusChem*, 2021, **14**, 595–613.

36 W. Sha, Y. Guo, D. Cheng, Q. Han, P. Lou, M. Guan, S. Tang, X. Zhang, S. Lu, S. Cheng and Y.-C. Cao, *npj Comput. Mater.*, 2022, **8**, 223.

37 J. Zhao, W. Zhang, A. Huq, S. T. Misture, B. Zhang, S. Guo, L. Wu, Y. Zhu, Z. Chen, K. Amine, F. Pan, J. Bai and F. Wang, *Adv. Energy Mater.*, 2017, 7, 1601266.

38 P. Buffat and J. P. Borel, *Phys. Rev. A: At., Mol., Opt. Phys.*, 1976, **13**, 2287–2298.

39 A. Cao, R. Lu and G. Veser, *Phys. Chem. Chem. Phys.*, 2010, **12**, 13499–13510.

40 A. I. Persson, M. W. Larsson, S. Stenström, B. J. Ohlsson, L. Samuelson and L. R. Wallenberg, *Nat. Mater.*, 2004, **3**, 677–681.

41 M. Gu, I. Belharouak, A. Genc, Z. Wang, D. Wang, K. Amine, F. Gao, G. Zhou, S. Thevuthasan, D. R. Baer, J.-G. Zhang, N. D. Browning, J. Liu and C. Wang, *Nano Lett.*, 2012, **12**, 5186–5191.

42 P. Xiao, W. Li, S. Chen, G. Li, Z. Dai, M. Feng, X. Chen and W. Yang, *ACS Appl. Mater. Interfaces*, 2022, **14**, 31851–31861.

43 M. Wang, A. Elgowainy, U. Lee, A. Bafana, P. T. Benavides, A. Burnham, H. Cai, Q. Dai, U. R. Gracida-Alvarez, T. R. Hawkins, P. V. Jaquez, J. C. Kelly, H. Kwon, Z. Lu, X. Liu, L. Ou, P. Sun, O. Winjobi, H. Xu, E. Yoo, G. G. Zaimes and G. Zang, *Summary of Expansions and Updates in GREET*® *2020*, U.S. Department of Energy, Office of Scientific and Technical Information, Lemont, IL, USA, 2020.

44 Q. Dai, J. Spangenberger, S. Ahmed, L. Gaines, J. C. Kelly and M. Wang, *EverBatt: A Closed-loop Battery Recycling Cost and Environmental Impacts Model*, 2019.

5912 | *Energy Environ. Sci.*, 2025, **18**, 5902–5912

This journal is © The Royal Society of Chemistry 2025